Journal of Nuclear Materials 406 (2010) 175–186

Contents lists available at ScienceDirect

Journal of Nuclear Materials

journal homepage: www.elsevier.com/locate/jnucmat

Overview of the RPV-2 and INTERN-1 packages: From primary damage to microplasticity

G. Adjanor [a,*], S. Bugat [a], C. Domain [a], A. Barbu [b]

[a] EDF Research and Development Division, Dpt. Matériaux et Mécanique des Composants, Les Renardières, F-77818 Moret-sur-Loing Cedex, France
[b] CEA, DEN, Service de Recherches de Métallurgie Physique, F-91191 Gif-sur-Yvette cedex, France

A B S T R A C T

In the framework of the European project PERFECT, four multiscale simulation packages dedicated to the prediction of evolution of material properties were developed. Among them, the RPV-2 and INTERN-1 are two simulation sequences of similar structure dealing with radiation damage in the reactor pressure vessel and the reactor internal structures, respectively. Both start at the atomic scale, where the neutron spectrum of the specified reactor is used to determine the energy distribution of the primary knocked-on atoms (PKA). A database of molecular dynamics results is then used to integrate the instantaneous production of defect clusters resulting from the displacement cascades initiated by each PKA. Depending on the type of calculation chosen to model long-term diffusion and reactions of defect clusters, precipitates and mixed-clusters, this primary damage enters either in rate equations or in Object Kinetic Monte Carlo simulations. The later correspond to a more accurate (but also more computationally demanding) physical model for diffusion as positions of objects on a lattice are explicitly treated. Finally, the increase of critical resolved shear stress is estimated from these cluster distributions either using an analytical model, taking into account the self and mutual dipole interactions of dislocations pinned on randomly dispersed unshearable obstacles, or by simulating the glide of a single dislocation line in its main slip system. Dislocation dynamics simulations were already used to validate some of the assumptions of the latter models, and will be fully integrated in the next versions of the packages.

1. Introduction

During their lifetime, reactor components have their physical properties modified due to irradiation. Among critical components, the reactor pressure vessel (RPV) is a matter of great attention as it cannot be replaced and thus conditions the lifetime of the whole nuclear plant. The usual assessment of the mechanical properties of reactor pressure vessels is traditionally based on the extrapolation of semi-empirical formulas, which are fitted on surveillance program data. For the concern of plant lifetime extension, simulations could be a valuable support to extrapolations. This requires a comprehensive physical modelling of the induced hardening and embrittlement. From the elementary physical processes generating the radiation damage to the evolution of the mechanical properties under irradiation a large range of length and time scales is covered. As a consequence, the simulation tools allowing to achieve this goal can only be a multiscale sequence of simulation codes. This includes the development of the numerical or theoretical tools and the experimental validation at the relevant scale. Seminal work to create an integrated tool taking into account the impact of reactor neutron spectrum on the production of defects affecting the microstructure was started in the REVE (REactor for Virtual Experiments) initiative [1–3]. From this initiative it appeared that the follow-up of the project had to reduce the empiricism of the models using specific experimental data to calibrate and validate some of the models present in the codes. It also appeared that the packages had to be integrated in a flexible platform to allow the comparison of different types of multiscale sequences involving different types of simulations. In the framework of the European project PERFECT, a new package called `RPV-2` was built following a scheme similar to that of `RPV-1` but with more possibilities, and integrating better assessed codes thanks to the improvements in the physical modelling and to calibration on dedicated experiments. The same scheme was also used to build a first prototype of `INTERN-1`, a multiscale package dedicated to internals ageing processes such as hardening and swelling.

In this article, we describe the common features of `RPV-2` and `INTERN-1` and give a elementary overview of the simulation codes integrated and their underlying physics. For extensive technical details on the codes, the reader should refer to their respective documentations (which are provided within `Perspycace` [4], the graphical user interface allowing to operate three end-products

* Corresponding author. Tel.: +33 160736697; fax: +33 160736889.
E-mail address: gilles.adjanor@edf.fr (G. Adjanor).

0022-3115/$ - see front matter © 2009 Elsevier B.V. All rights reserved.
doi:10.1016/j.jnucmat.2009.09.006

of the PERFECT platform: RPV-2, INTERN-1 and ToughnessModule [5]) and to the comprehensive suite of articles of this special edition. An overview of the RPV-2 package is given on Fig. 1. Its first module, IRRAD, uses the SPECTER code to evaluate the PKA (primary knocked-on atom) spectrum from a given neutron spectrum. The second operation is to convolve this PKA spectrum with a database of cascades, to obtain the instantaneous defect cluster production resulting from this spectrum. In the CONVOLVE module, this computation is made on the basis of an almost linear correspondence between the defect production due to cascades of a specific energy level and PKA spectrum. The database of cascades is produced by molecular dynamic simulations (MD), with an accurate interatomic potential (Fe–Cu [6] for RPV steels, or Fe–Ni for internals [7]), taking into account at most one chemical element

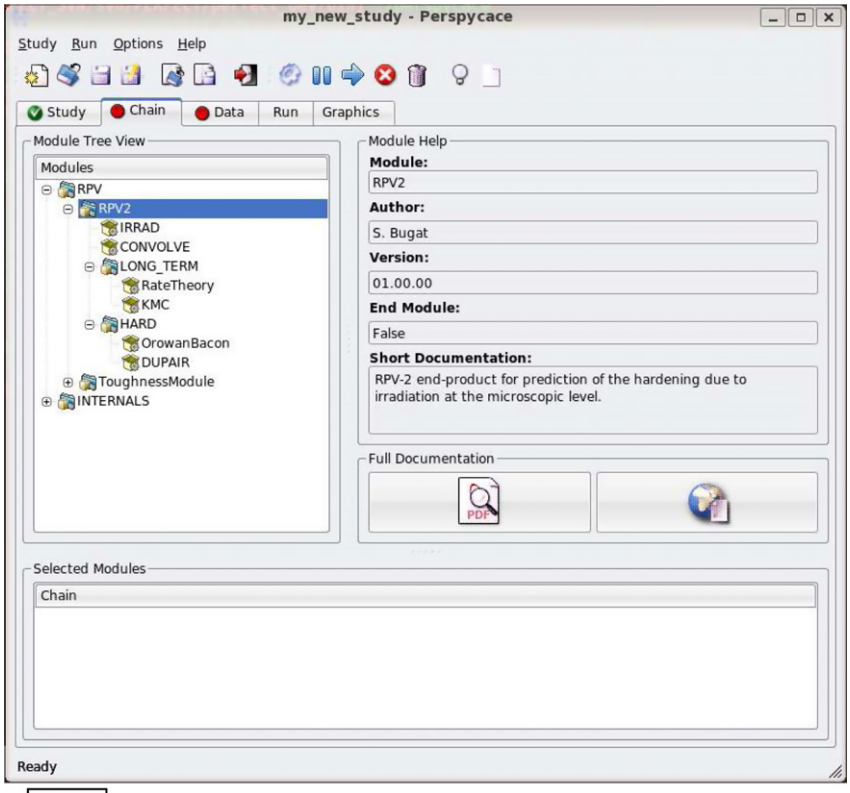

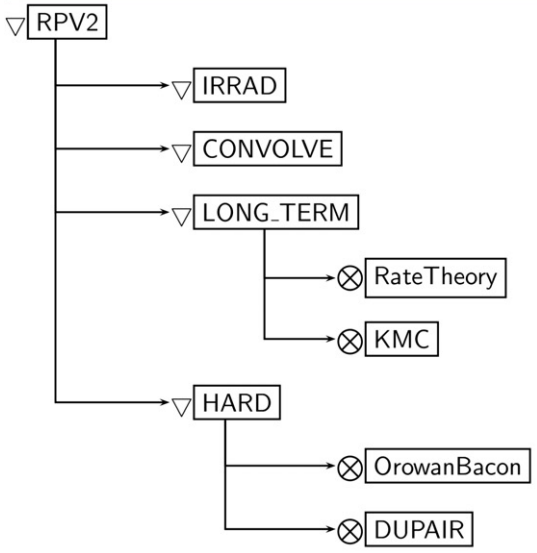

Legend:

⊗ = "or" (choice between sub-modules)

▽ = "and" (chaining of sub-modules)

Fig. 1. Top: caption of the Perspycace interface allowing to operate RPV-2, INTERN-1 and the Toughness module. Bottom: tree-view of the RPV-2 showing the sequence of modules that constitute the package (triangles) and the submodules to be chosen for the LONG_TERM and HARD. The prototype version of INTERN-1 shares the same structure except for KMC and DUPAIR modules which are only integrated in RPV-2.

that can have an impact on the structure of the cascades. The evaluation of the long-term fate of the defects (up to 40 years for both internals and RPV steels) is then done with the help of the LONG_TERM module. The LONG_TERM module offers the possibility to use either a rate-theory or an object kinetic Monte-Carlo code to take into account the most important solute species, that is helium (He) for internals and copper (Cu) for RPV steels. The output of the LONG_TERM module is the distribution (size and density) of defect clusters, precipitates and mixed clusters including defects and solute atoms. To estimate the increase of critical resolved shear stress due to the pinning of these defects on gliding dislocations, the HARD module will use either an analytical formula for dipole interactions of randomly dispersed obstacles or a simplified single dislocation 2D glide simulation based on the Foreman and Makin formalism [8]. From these results, the hardening and ductile to brittle transition temperature shift can be computed with the use of the ToughnessModule which is presented in a separate article of this issue [5].

2. Computing the PKA spectrum with the IRRAD module

In order to estimate the primary damage resulting from a given reactor spectrum, the first step is to compute the PKA spectrum. In the current version of RPV-2 this is done with the use of the SPECTER [9,10] code delivered by NEA (Nuclear Energy Agency). At the atomistic level, neutron irradiation collisions with atoms of the host material produces reaction products and recoil atoms, the PKA. The PKA loose part of the kinetic energy they received by generating electronic excitations as they interact with the electronic density of the host material atoms, and they may also interact with other atoms of the host material by elastic and inelastic collisions. These collisions can result in permanent displacement of atoms, which is measured by the displacement per atom (dpa).

In order to estimate the dpa-rate (dpa per unit time) and the PKA spectrum (instantaneous density of PKA for given energy), one has to provide a so-called "grouped" neutron spectrum Φ (in number of neutrons per unit surface and time) as a function of the neutron energy E in eV in the form of couples of values (E_i, Φ_i):

$$\Phi_i = \int_{E_i}^{E_{i+1}} \frac{d\phi}{dE} dE, \tag{1}$$

where $\frac{d\phi}{dE}$ is the so called differential neutron flux. Yet, for the sake of simplicity, $\Phi(E)$ will designate an appropriate grouped neutron spectrum, and sums over groups will not appear in the following formulas.

In the SPECTER code the main kinds of neutron–atom interactions are taken into account:

- elastic scattering (no conversion of mass into energy), which is the dominant process especially at low neutron energy [9], is treated exactly including angular distributions from cross-sections database ENDF/B-V,
- inelastic scattering calculations are treated exactly in the resolved domain (except for angular distributions which are considered isotropic) and approximated with an evaporation model in the unresolved domain,
- multiple particle reactions such as (n, xn) (re-emissions of x neutrons) are taken into account by a Monte-Carlo sampling of the secondary recoil distributions,
- radiative capture ((n, γ) reaction) events are also considered,
- gas production and especially α decay can also be computed, which will be of greater interest in the case of internals, where nickel transmutes to iron by α decay,
- beta decay eventually coupled with γ emission.

The PKA density η as function of PKA energy E_{PKA} can be expressed as follows:

$$\eta(E_{\mathrm{PKA}}) = \rho \sum_k \int_{E_{\min}}^{E_{\max}} \Phi(E_n)\sigma_k(E_n, E_{\mathrm{PKA}}) dE_n, \tag{2}$$

where $\rho = 1/V_{\mathrm{at}}$ is the atomic density of the host material, k is the reaction channel (i.e. the type of neutron–atom reaction considered), $E_{\min}$ and $E_{\max}$ are, respectively, the minimum and maximum energy transferred in the collision ($E_{\max} = 20$ MeV for SPECTER as cross section data files stop at this value). The differential cross-section $\sigma_k(E_n, E_{\mathrm{PKA}})$ represents the probability that a lattice atom interacting with a neutron of energy E_n results in a transfer of energy E_{PKA} to the struck atom.

3. Retrieving the NRT-dpa rate from the PKA spectrum

The Kinshin and Pease function, whose expressions is recalled in the Appendix A, allows us to define the dpa according to the definition of Norgett, Robinson, and Torrens [11] (the "NRT" dpa), which is the damage measure used for engineering applications as recommended by the ASTM [12] (American Society for Testing and Materials). For a given PKA energy E_{PKA}, the NRT-dpa is conventionally defined as:

$$dpa_{\mathrm{NRT}}(E_{\mathrm{PKA}}) = \frac{\kappa E_{\mathrm{dam}}(E_{\mathrm{PKA}})}{2E_D}, \tag{3}$$

where κ is a constant equal to 0.8. This formula bears the following physical interpretation: if we assume that an initial PKA will completely transfer its damage energy $E_{\mathrm{dam}} = \xi E_{\mathrm{PKA}}$ (see Appendix B) to two secondary atoms, and that each of these two secondary atoms will again transfer their energy to two tertiary atoms, and so on, this process models a simplified cascade which ends up at the cascade stage where the transferred energy becomes lower than the threshold energy E_D in the host material. As a consequence, the ratio $\frac{E_{\mathrm{dam}}}{2E_D}$ represents the number of atoms displaced at the end of this cascade process.

The NRT-dpa rate (also called NRT damage rate) for the whole PKA spectrum can be expressed by the following formula:

$$G_{\mathrm{NRT}} = \frac{dpa_{\mathrm{NRT}}}{t_{\mathrm{irrad}}} = \frac{1}{\rho} \int \frac{\kappa E_{\mathrm{dam}}}{2E_D} \eta(E_{\mathrm{PKA}}) dE_{\mathrm{PKA}}, \tag{4}$$

Identifying the NRT-dpa definition with the Kinshin and Pease function allows us to define the NRT-dpa cross-section:

$$\sigma_{\mathrm{dpa}} = \frac{\int \Phi(E_n)\sigma_{\mathrm{DIS}}(E_n) dE_n}{\int \Phi(E_n) dE_n}, \tag{5}$$

where σ_{DIS} is a displacement cross-section defined in Appendix A. This definition allows us to give an order of magnitude of the NRT-dpa for typical typical pressurized water reactors (PWR) end-of-life conditions. For technological purpose, the dpa cross-section is often defined as:

$$\sigma_{\mathrm{dpa}} = \frac{dpa_{\mathrm{NRT}}}{\int_{E_n > 1MeV} \Phi(E_n) dE_n t_{\mathrm{irrad}}} \tag{6}$$

and is typically equally to 1500 barn [13,14], quite independently of the considered ferritic alloy of the neutron spectrum used. For typical PWR end-of-life conditions, the targeted fast neutron fluence ($\int_{E_n > 1\ \mathrm{MeV}} \Phi(E_n) dE_n t_{\mathrm{irrad}}$) is about 6.5 $10^{19} n\ \mathrm{cm}^{-2}$ [15] which gives a value typical of 0.1 dpa_{NRT} for RPV-steels (several tens of NRT-dpa for internals, depending on the location).

4. Estimating the effective dpa from the cascade database of CONVOLVE

As stated before, the definition of the NRT-dpa relies on a very simplified model of cascade formation (the Kinshin and Pease model) that will clearly overestimate the number of displaced atoms through the cascade development process. A much more realistic estimate of the actual values taken by $\nu(E_{\mathrm{dam}})$ can be found using molecular dynamics simulations (MD). The cascade evolution consists of three main stages:

(i) The PKA atom with an initial kinetic energy E_{dam} leads to the formation of the cascade and its spatial expansion (typically a picosecond for iron [16]) with a large number of defects.
(ii) During the second stage, called in intra-cascade recombination stage, most of the defects created recombine and some vacancies and interstitials remain in the cascade area (typically ten to few tens of picoseconds) to form the primary damage, called "raw cascade" (illustrated in Fig. 2). This recombination process takes place much faster that it would at the equilibrium temperature $T = T_{\mathrm{irrad}}$. This is due to the diffusion of the damage energy to the atoms of the system, in fact the cascade coincides with a thermal spike that will enhance diffusion and recombination processes before equilibrating with surrounding atoms and finally transferring its heat to the whole system.
(iii) The third stage corresponds to the evolution of these defects by thermal diffusion and even if some vacancies and interstitials are very close to each other, the time scale for clustering or recombinations will be much larger. Here, the use of a kinetic Monte-Carlo procedure (KMC) will allow us to simulate diffusion processes on a much larger timescale than MD, as each step of the simulation corresponds to a migration event. The simulations must be stopped as soon as a defect goes out of the simulation box. In fact, as the box dimension has been chosen to approximately match the inverse of the typical cascade densities in the material, when a defect goes out of the box not only "intracascade" but also "intercascade" recombination processes may occur. From this stage the KMC annealing process (in fact the system is maintained at T_{irrad} rather than "annealed") of a single cascade becomes irrelevant, and must thus be stopped. After, typically, some milliseconds, about 30% of the total amount of Frenkel pairs have recombined during the annealing stage in the case of iron [17]. The cascades obtained by this process are referred to as "annealed cascades", and will be of great importance in the case of rate-theory simulations, which, because of their use of a mean field approach, do not take into account defect spatial positions, but concentrations of defects in an equivalent homogeneous medium. As a consequence, the damage due to a Frenkel pair whose elements are close to each other is strongly overestimated, as the pair has a high probability to recombine. Calculating the damage rate from an annealed cascade database can improve the accuracy of this source for rate-theory calculations as defect densities tend to homogenize after short term diffusion.

4.1. Applying MD cascade simulations to the PKA spectrum

In principle, one should simulate displacement cascades for every damage energy of the PKA spectrum. In practice, simulations with the TRIM code gave numerical evidence [1] and the INCAS model [18] gave precise theoretical justification that cascades produced by high energy PKA split almost linearly into sub-cascades. Indeed, for high PKA energies, where the binary collision approximation (BCA) holds, the mean free path between two high energy collisions (which is proportional to the inverse cross-section) is large compared to the cascade extension, sub-cascades are thus formed [16]. Fig. 3 from Stoller et al. [19] illustrates the formation of subcascades into 40, 20 and 10 keV cascades.

The idea of the CONVOLVE module is to store in a database a set of varying energy MD-cascades (for example 40, 20 and 10 keV cascades) for different temperatures and alloying element content, and to decompose the damage energies spectrum given by the list $(E^i_{\mathrm{dam}}, \eta^i)$ onto the referential of energies of the considered cascade database. Namely, let us denote by $E^k_{\mathrm{MD-DB}}$ the different damage energies available in the database. A given damage energy E^i_{dam} can be projected onto this base using the following rule:

$$E^i_{\mathrm{dam}} = \sum_{k=1}^{m} \alpha_{ik} E^k_{\mathrm{MD-DB}} + \Delta E^i \tag{7}$$

All α_{ik} have to be positive (or null) integers. To compute the α_{ik}, the following iterative procedure is used: if m is the maximum indice so that $E^m_{\mathrm{MD-DB}} \leqslant E^i_{\mathrm{dam}}$, α_{im} is the Euclidian division of both terms: $\alpha_{im} = E^i_{\mathrm{dam}}/E^m_{\mathrm{MD-DB}}$. Then the preceding term $\alpha_{i(m-1)}$ is computed using the same procedure: $\alpha_{i(m-1)} = [E^i_{\mathrm{dam}} - \alpha_{im} E^m_{\mathrm{MD-DB}}]/E^{m-1}_{\mathrm{MD-DB}}$. And finally any $\alpha_{i(k-1)}$ is computed from the others according to:

$$\alpha_{i(k-1)} = \left[E^i_{\mathrm{dam}} - \sum_{p=k}^{m} \alpha_{ip} E^p_{\mathrm{MD-DB}} \right] \Big/ E^{k-1}_{\mathrm{MD-DB}}. \tag{8}$$

This decomposition can be done on whatever chosen raw or annealed cascade database. The $E^k_{\mathrm{MD-DB}}$ energies are listed by selecting first the closest temperature in the database from the irradiation temperature.

For the annealed database, the closest copper content in the database from the actual copper content of the material is also se-

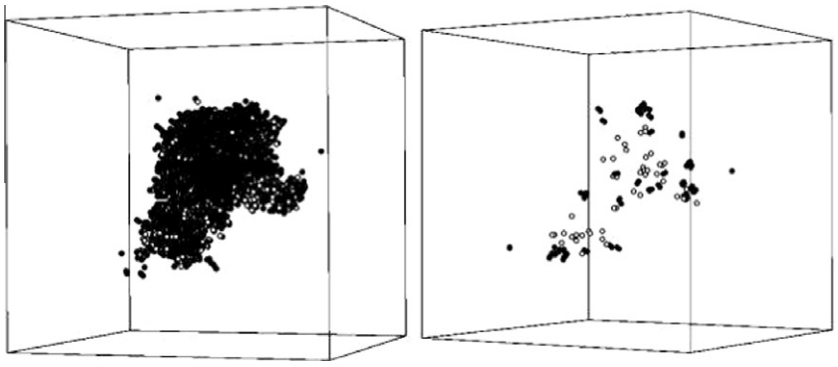

Fig. 2. Residual defects of a 20 keV cascade in iron in a 20 nm box at the end of the quenched stage. On the right hand image, the light colored circles represent vacancies and the dark colored ones interstitial atoms. The left-hand image represents not only the defects but also atoms displaced during the replacement sequence.

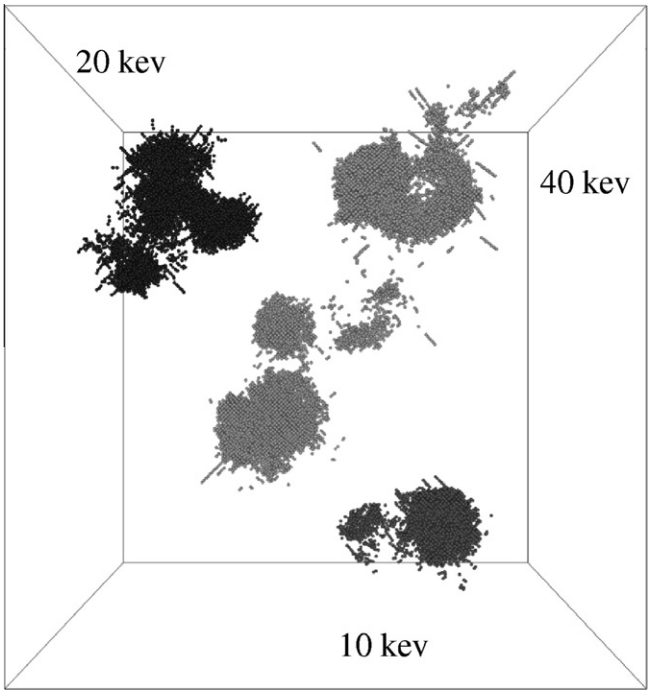

Fig. 3. Subcascades in α iron at 100 K [19] for a 40, 20 and 10 keV cascade. All the displaced atoms through the replacement sequence are represented.

lected. The last step is to compute the densities associated with each damage energy of the database (raw or annealed) $E^k_{\mathrm{MD-DB}}$. Let us denote by η^k_{casc} theses densities. Coming from the above equations, we have directly:

$$\eta^k_{\mathrm{casc}} = \sum_i \eta_i \alpha_{ik}. \tag{9}$$

Finally, for a given cascade database, we obtain an equivalent cascade spectrum which is characterized by $(\eta^k_{\mathrm{casc}}, E^k_{\mathrm{MD-DB}})$. In practice, cascade energies are sampled by 10 keV PKA energy range, thus PKA for lower energies than 10 keV are assumed to produce only Frenkel pairs, whose number is evaluated thanks to the Bacon–Calder model [20]. This model is used to estimate the number of Frenkel pairs due to the residual energies resulting from the former decomposition:

$$\nu_1^0 = \alpha \Delta E^{i\beta} \tag{10}$$

Identified values $\alpha = 5.67$ and $\beta = 0.779$ fit very well MD data for bcc iron at 100 K [19,21] and are assumed to be valid at higher temperatures.

Now, if we denote by ν^k_n the average number of clusters of size n ($n \geqslant 1$ for interstitials and $n \leqslant -1$ for vacancies) in the cascade of energy $E^k_{\mathrm{MD-DB}}$, then the source term can be expressed as follows:

$$G(n) = \sum_{k=0}^{m} \eta^k_{\mathrm{casc}} \nu^k_n. \tag{11}$$

The source term or primary damage $G(n)$ represents the number of clusters of size n contained in all the cascades induced by the considered neutron spectrum per unit volume and unit time. Roughly, it should be a fast decreasing function of n, and mono-defects should represent about 50% of the source term. Integrating $nG(n)$ gives us an estimate of the total MD dpa-rate resulting from the considered damage spectrum, which represents the equivalent amount of surviving Frenkel pairs:

$$G_{\mathrm{MD}} = \sum nG(n), \tag{12}$$

this sum being equivalently done on vacancies or interstitials as their number is equal. For the sake of accuracy, all cascade databases have been averaged on several thousands of runs and using at least three different initial PKA momentum directions. Presently, four cascade databases for RPV obtained in Fe and Fe–Cu using different potentials at different temperatures are integrated in `RPV-2`.

Once an irradiation temperature is chosen, the `CONVOLVE` module chooses the nearest temperature in the database. A similar interpolation is eventually done for the copper content if the cascade database chosen contains different copper concentrations. Nevertheless, as the study related to these calculations [6] has shown that for typical RPV copper contents, copper atoms had a weak influence on the cascade morphologies, the RPV-2 database does not take into account copper content anymore at this level. Concerning `INTERN-1`, the situation is quite different: the effect of the 10—15$\%_{\mathrm{at}}$ Ni must be taken into account to accurately consider the cascade morphology. Unfortunately the austenitic material is a concentrated complex alloy and it is modelled by a binary Fe–Ni alloy to simulate the cascades. As important solute atoms, such as Nitrogen, that stabilize the face centered cubic (fcc) Fe–Ni structure are not modelled, below 35$\%_{\mathrm{at}}$ nickel, PKA atoms destabilize the metastable fcc structure which is turned into a body centered cubic structure. For that reason, at the current state of `INTERN-1`, an "equivalent" nickel content greater or equal to 35$\%_{\mathrm{at}}$ must be chosen.

Depending on the empirical potential which the database relies on, the ratio $G_{\mathrm{NRT}}/G_{\mathrm{MD}}$ will approach 3, confirming that the NRT-dpa strongly overestimates the actual damage produced by irradiation.

5. Modelling diffusion processes and the long-term fate of defect distributions

Defect clusters yielding from the cascade process will completely change the nature of the diffusion processes occurring in the host material. Indeed, diffusion in a crystalline solid under irradiation is quite different from the unirradiated case. In the unirradiated case, diffusion is ensured by mono-vacancy jumps, and the interstitials have a high formation energy (typically between 3 and 6 eV) that prevents them from having a significant equilibrium concentration, and moreover their lower migration energy make the very few interstitials disappear almost instantaneously at the interfaces at room temperature. Their contribution to diffusion processes at equilibrium is thus completely negligible. Under irradiation, as stated before, cascades produce large amounts of spatially correlated (i.e. with close lattice positions) Frenkel pairs which can aggregate to form defect clusters. As a consequence the concentration of produced interstitials is large (several orders of magnitude higher than equilibrium concentration of vacancies, the crystal is thus said to be super-saturated) and it is equal to the concentration of produced vacancies, as, at this stage, both type of defects can only be produced or destroyed by Frenkel pair recombinations. Thus both vacancies and interstitial clusters can significantly contribute to diffusion processes under irradiation. This can impact the microstructure in three ways:

- mobile defect clusters can favor the growth of cavities or interstitial type dislocation loops ("matrix damage"). Indeed distributions of dislocation loops are clearly visible in transmission electron microscopy on pure iron.
- super-saturated mobile defect clusters will also enhance inter-diffusion processes. Among the main alloying elements (Ni, Mn,Si ,Mo) and impurities (Cu, P) of RPV-steels, copper is most significant for embrittlement concerns. The solubility limit of copper in iron is extremely low (about $4.8 \times 10^{-3}\%_{\mathrm{wt}}$ [22]), as

a consequence, RPV-steels are always super-saturated with copper (even if copper levels are low by careful control of recycling of scrap). In the unirradiated case, the nucleation of equilibrium copper precipitates is kinetically blocked at usual temperatures, but this is not the case under irradiation. For high copper content ($P_{Cu} > 0.3\%$wt), it was clearly shown that copper precipitates are formed by irradiation accelerated homogeneous precipitation [23]. In this case, the process is exactly the same as in the unirradiated case, except that the coefficient D_{irrad} is greatly enhanced, at least proportionally to the mono-vacancies super-saturation $\frac{C}{C_{\text{eq}}}$ as a first approximation: $D_{\text{irrad}} = D_{\text{th}}\frac{C}{C_{\text{eq}}}$ [24,25]

- for lower copper content ($P_{\text{Cu}} < 0.1\%$wt) as is the case for the French RPV steel, it was shown indirectly [26–29] that this irradiation-accelerated homogeneous precipitation does not hold, and that copper precipitates formed must be due either to heterogeneous precipitation on defect clusters or to induced segregation, i.e. coupling between fluxes of defects to the sinks and solute atoms fluxes. In either cases, the mobility of mixed defect clusters must be explicitly taken into account in the equations describing the long-term fate of defects.

5.1. The rate-theory submodule

Rate-theory codes such as MFVISC are based on a mean-field approach that reduces the modelling of defects and solute atoms diffusion under irradiation to the solving of a system of coupled ordinary differential equations, the rate kinetic equations. The mean-field approximation consists here in considering an effective homogeneous medium in which concentrations C of defect clusters are considered and all diffusion processes occur continuously in time and space. The spatial correlation between objects is not considered explicitly (see [30] for an introduction on rate-theory).

In MFVISC one considers the concentrations $C(n,p)$ of defects from the various classes (n,p), where n is a relative integer denoting the number of self defects (positive n indicates a number of n self-interstitials, negative n stands for n vacancies) and p is a positive integer standing for the number solute atoms (copper atoms for RPV-2 and helium for INTERN-1) in the cluster.

Simulating the diffusion processes in irradiated materials essentially consists in estimating the rate at which mobile defects will be captured or emitted by existing clusters. Each capture or emission will make the clusters grow or shrink. In MFVISC, defect clusters with $m_v \leqslant n \leqslant m_i$ (depending on their interstitial or vacancy type) and $p = 0$, as well as $n = \pm 1$ and $p = 1$ are considered as mobile. The absorption coefficient $B((n,p),(m,q))$ corresponds to the capture of a cluster of type (m,q) by a cluster (n,p):

$$(n,p) + (m,q) \overset{B((n,p),(m,q))}{\rightarrow} (n+m, p+q).$$

Of course, in the specific case where, $p = q = 0, n = -m$, the reaction is a recombination. In the case of emission reactions, we consider the following emission coefficients A:

$$(n,p) \overset{A((n,p),(1,0))}{\rightarrow} (n-1,p) + (1,0), \quad \text{for } n \geqslant 2$$
$$(n,p) \overset{A((n,p),(-1,0))}{\rightarrow} (n+1,p) + (-1,0),$$
$$(n,p) \overset{A((n,p),(1,1))}{\rightarrow} (n-1,p-1) + (1,1), \quad \text{for } n \geqslant 2$$
$$(n,p) \overset{A((n,p),(-1,1))}{\rightarrow} (n+1,p-1) + (-1,1)$$

Most of the features of a given rate-theory model are contained in the expression of the absorption and emission coefficients and sink strengths. In the case of the capture of cluster (m,q) by a cluster of (n,p), it is assumed that the capture coefficient can be deduced from the diffusion equation at the stationary state. The diffusion equation is solved for $\partial C/\partial t = 0$ and we model the cluster (n,p) as a spherical sink by imposing the following boundary conditions to the diffusion equation: the concentration of cluster (m,q) is zero at the capture radius $r^*((n,p),(m,q))$, the interface between the cluster and the medium, and the concentration is $C(m,q)$ at infinite radius. Integrating the (m,q) clusters flux through the sphere of radius $r^*((n,p),(m,q))$ yields:

$$B((n,p),(m,q)) = 4\pi r^*((n,p),(m,q))[D(n,p) + D(m,q)], \tag{13}$$

where $D(n,p) = D_0(n,p)\exp\left(\frac{-E_m(n,p)}{k_B T}\right)$ and $D(m,q)$ are the diffusion coefficients of clusters (n,p) and (m,q), respectively, (diffusion coefficients are zero if clusters are immobile). Diffusion coefficients are given by the Arrhenius law: $D(n,p) = D_0(n,p)\exp\left(\frac{-E_m(n,p)}{k_B T}\right)$, where D_0 is the prefactor, and $E_m(n,p)$ is the migration energy of the cluster (n,p), calculated *ab initio* [31–33]. The capture radius is usually written as:

$$r^*((n,p),(m,q)) = Z(n,m)(r^*(n,p) + r^*(m,q)), \tag{14}$$

where $Z(n,m)$ is the bias factor, accounting for the phenomenological bias on the interstitial and vacancy capture radii due to their different elastic fields. In MFVISC, as the model is already quite complex due to the treatment of mixed clusters, the most simple expression for the capture radii have been taken: the term $(r^*(n,p) + r^*(m,q))$ in Eq. (14) is replaced by $(R(n,p)+R(m,q)+R_0)$, where the first two terms are the equivalent spherical radii of the clusters and R_0 is a constant. Using the spherical radius in the expression of all capture radii, implies that all clusters are considered as spherical, including interstitial clusters, which are observed to be $\langle 100\rangle$ or $\langle 111\rangle$ interstitial dislocation loops according to the irradiation conditions [34]. Moreover, the bias factor is taken as $Z(n,m) = Z_i$ if n and m are positive and $Z(n,m) = 1$ in the other case. As using realistic expressions for the bias factor and for the capture radius of an interstitial loop mixed with copper precipitates would require a dedicated study, the choices made for the current parameterization of the code must be considered as first approximations. In the case of emission the expression of the coefficients contains a Boltzmann factor accounting for the probability to break the binding between $(n-m,p-q)$ and (m,q), whose associated energy is in fact noted $E_b((n,p),(m,q))$ and also contains an absorption term $B((n-m,p-q),(m,q))$ as the defect must be emitted beyond the capture radius:

$$A((n,p),(m,q)) = B((n-m,p-q),(m,q))\frac{1}{V_{\text{at}}} \times \exp\left(\frac{-E_b((n,p),(m,q))}{k_B T}\right), \tag{15}$$

where V_{at} is the atomic volume. As only isolated point defects and defect-solute pairs can be emitted, $(m,q) = (\pm 1, 0|1)$ (we note 0|1 zero or one). Again the binding energies for small mixed clusters have been calculated *ab initio*, except for large clusters where an expression fitted on MD calculations from Kulikov et al. [35] is used.

The last type of reaction that must be considered is the interaction with fixed sinks such as dislocations and grain boundaries. In MFVISC, the sink strength for dislocations is modeled by: $L_d(n,p) = \rho_d Z_\alpha D(n,p)$ where ρ_d is the dislocation density, while in the case of grain boundaries, the sink strength is given by $L_{gb}(n,p) = 6\frac{K_s(n,p)}{l}$, where l is the grain size and the K_s coefficient is related to the sum of the sink strengths of all defects. Note that saturation effects that hold in the case of climbing are not taken into account in the dislocations sink strengths.

To describe the time evolution of the concentration $C(n,p)$, we must consider the following set of rate equations:

$$\begin{aligned}\frac{\partial C(n,p)}{\partial t} &= G_{\mathrm{MD}}(n) - A((n,p),(1,0|1))C(n,p) \\ &\quad - A((n,p),(\bar{1},0|1))C(n,p) + A((n+1,p),(1,0|1)) \\ &\quad \times C(n+1,p) + A((n-1,p),(\bar{1},0|1))C(n-1,p) \\ &\quad + \sum_{m=1}^{\min(n-No\upsilon,m_\upsilon)} \sum_{q=0}^{1} B((n-m,p-q),(m,q))C(n-m,p-q) \\ &\quad \times C(m,q) + \sum_{m=1}^{\min(Noi-n,m_i)} \sum_{q=0}^{1} B((n+m,p-q),(m,q)) \\ &\quad \times C(n+m,p-q)C(m,q) - \sum_{m=-m_\upsilon,m\neq 0}^{m_i} \sum_{q=0}^{\min(1,p)} B((n,p),(m,q)) \\ &\quad \times C(n,p)C(m,q) - \mathbb{1}_{-m_\upsilon\leqslant n\leqslant m_i \text{ and } p\leqslant 1} B(n,p,n,p)[C(n,p)]^2 \\ &\quad - L_{gb}(n,p)C(n,p) - L_d(n,p)C(n,p), \end{aligned} \tag{16}$$

where $\mathbb{1}_{-m_\upsilon\leqslant n\leqslant m_i \text{ and } p\leqslant 1}$ equals 1 for a mobile (n, p) cluster, and else 0. The terms appearing in the sum bounds, will be defined further. This simplified equation expresses the balance between positive contributions and negative contributions to the growth rate of class (n, p):

- a positive contribution due to the clusters of size n from the source term $G_{\mathrm{MD}}(n)$,
- (n, p) clusters emitting a single defect (or a defect-solute atom pair) go out from the class, which results in a negative contribution to concentration derivative,
- a positive contribution rises from $(n \pm 1, p)$ and $(n \pm 1, p + 1)$ clusters emitting a single defect or defect-solute atom pairs, respectively, which results in a production of (n, p) clusters,
- a positive contribution from the absorption if two clusters merge into a new (n, p) cluster,
- a negative contribution from the absorption if an (n, p) merges with another cluster belonging to another cluster class. Note that the term $\mathbb{1}_{-m_\upsilon\leqslant n\leqslant m_i \text{ and } p\leqslant 1}$ is needed to correct the sum of absorption terms when $m = n$ because the reaction of an (n, p) cluster with another (n, p) cluster will consume two (n, p) clusters,
- a negative contribution from fixed sinks: grain boundaries and dislocations absorbing part of the mobile clusters.

Writing down all the rate equations for large enough values of n and p can result in a huge system of coupled differential equations. Indeed experimental measurements show that concentrations of clusters with very high values of n (several hundreds of thousands) and high values of p (several hundreds) should be computed. If one equation for each possible couple of (n, p) values was necessary, the solving of this system would be impossible with current computer resources. Nevertheless, this is quite easily achieved for very large values of n, by using the Fokker–Planck formalism and casting the rate equations with n replaced by a continuous variable x for large values of n. Discrete equations are kept for values of n lower than $No\{i, \upsilon\}$ in Eq. (16). And for the continuous treatment, the incremental values of x (Δx) increase with the index of the equation and typically reach several hundreds of thousands for the last equation. In the case of variable p, it turns out that it is not trivial to solve the rate equation when using continuous variables for both n and p. Thus as the equations can only be solved for discreet values of p, the maximum number of copper atoms that can be considered in the cluster, *Nob* is quite small, typically about 20 or 30 is the maximum that can be run on a computer with 2 Gb RAM. This is strong limitation of the current version of the code because tomographic atom probe measurements suggest that mixed precipitates contain several hundreds of copper atoms. In practice, an MFVISC calculation with an insufficient value of *Nob* for given irradiation conditions will result to an underestimation of the solute cluster distribution (related to a non conserved copper concentration). Nevertheless, the treatment of mixed clusters done in MFVISC is an important achievement in the PERFECT approach which consists in reducing the empiricism of the models. Indeed for the first time, the copper heterogeneous segregation is treated explicitly. The use of other resolution methods and the parallelization of the code may allow to treat larger solute-defect clusters.

The main outputs of the MFVISC calculation are the cluster densities $C(n, p)$ time evolution.

Note also that some convenient quantities are provided to ease the comparison with experimental results:

- the defect size density, $F(R) = \frac{4\pi R^2}{V_{\mathrm{at}}} C(n,p)$ as a function of the cluster spherical radius $R(n + p)$ is also given,
- the cluster mean radii, $\frac{\int_{R>R_{\min}} RF(R)dR}{\int F(R)dR}$ where $R_{\min}$ is the experimental detection limit of the technique whose results will be compared to simulation,
- the mean number of atoms per cluster,

$$\frac{\int_{(n+p)\geqslant n_{\min}} (n+p)C(n,p)dndp}{\int_{(n+p)\geqslant n_{\min}} C(n,p)dndp}, \tag{17}$$

  where $n_{\min} = \frac{1}{V_{\mathrm{at}}} \frac{4\pi}{3} R_{\min}^3$
- the cluster number density,

$$\int_{(n+p)\geqslant n_{\min}} C(n,p)dndp. \tag{18}$$

5.2. The KMC submodule

The KMC submodule is an interface to the object kinetic Monte-Carlo code LAKIMOCA [17]. Contrary to the case of rate-theory, in an OKMC simulation, we explicitly consider the position of defect clusters on a lattice. To be more precise, only the position of the center of mass of objects is considered, while their spatial extent is replaced by a capture radius, that is calculated in the same way as in rate-theory. However, aggregation reactions will take place naturally if one of the two defects migrate and the distance between the two defects become smaller than the sum of the two capture radii. Migration events, which here correspond to jumps to neighboring lattice sites, are sampled according to the jump frequencies for an (n, p) cluster: $\Gamma_{n,p,l} = \nu(n,p)\exp(-\frac{E_m(n,p)}{k_B T})$, where $\nu(n, p)$ is the attempt frequency for event l. Emission events from traps or from objects follow the same law with E_m replaced by $E_m + E_b$.

In addition to the elements of the initial microstructure, such as grain boundaries, dislocations and traps (in an attempt to mimic the interactions of carbon on vacancies), irradiation is modelled by inserting as objects in the lattice the defects from raw cascades of energies $E^k_{\mathrm{MD-DB}}$ according to the cascade spectrum, with associated frequency:

$$P_k = \eta^k_{\mathrm{casc}} V_{\mathrm{box}}, \tag{19}$$

where V_{box} is simulation box volume.

Having defined the set of migration or emission events for all the objects as well as cascade events (which are summarized on Fig. 4), the OKMC procedure consists in selecting one of these events according to their respective frequencies. In LAKIMOCA, as the residence time [36] procedure is used to select the events, the time step increase Δt associated with the selected event is given by:

$$\Delta t = \frac{1}{\sum_{n,p,l}\Gamma_{n,p,l} + \sum_m P_m}. \tag{20}$$

As in the case of rate-theory, the substance of the physical model underlying an OKMC code is contained in the expressions capture radii, sink densities, migration energies and binding energies. These parameters can be modified in the `Perspycace` interface by a so-called "expert-user".

6. Estimating the increase of critical resolved shear stress with the HARD module

Within `RPV-2`, our final goal is to estimate the increase of critical resolved shear stress (CRSS) due to irradiation. With this output, the `Toughness module` can be used to estimate the resulting hardening and the ductile to brittle transition temperature shift [5]. The origins of the hardness in RPV steels are multiple and complex, the main contributions can be listed as follows [37]:

- τ_F, the lattice friction opposing to the dislocations mobility mainly due to the alloying elements in interstitial position such as carbon,
- τ_{forest}, the interactions of gliding dislocations with the forest of dislocations,
- $\tau_{carbides}$, the effect of dislocations pinning on carbides,
- $\tau_{confinement}$, includes the contribution of microstructural features which confine the dislocations: bainitic laths and grain boundaries (only the latter contribution is possibly altered by radiation induced segregation of substitutional elements),
- τ_{damage}, cavities, interstitial loops and precipitates and mixed precipitates eventually formed under irradiation.

Dislocation dynamics (DD) studies [37] support the assumption that the first four contributions are not affected by irradiation, as a first approximation. If we also assume that the resulting CRSS is simply the sum of the listed contributions (which will be further referred to as "linear mixture law"), we can thus estimate the increase of the critical resolved shear stress by:

$$\Delta\tau_c = \tau_c^{\text{irradiated}} - \tau_c^{\text{unirradiated}} \tag{21}$$

$$\simeq \tau_{\text{damage}} \tag{22}$$

where $\tau_c^{\text{irradiated}}$ and $\tau_c^{\text{unirradiated}}$ are the CRSS resulting from the composition of the listed contributions in the irradiated and unirradiated states respectively. The `HARD` module requires as input the cluster distributions from the `LONG_TERM` and will output the estimates of the increase of CRSS at the different output times chosen, using either an analytical formula for randomly dispersed unshearable precipitates with the `OrowanBacon` module, or simulating the 2D glide of a single dislocation through the cluster distributions, with the help of the `DUPAIR` submodule.

6.1. Analytical approach: the OrowanBacon submodule

There are very few models allowing to calculate analytically the CRSS due to obstacles (here defect clusters) in the gliding plane [38]. Assuming a constant line-tension, the well known Orowan formula [39], $\tau_{\text{Orowan}} = \alpha\frac{\mu b}{L}$, can be established for a dislocation segment bowing between an isolated pair of punctual impenetrable obstacles at a distance L and placed in a medium of shear modulus μ. The main approximation of this model is that it does not take into account the interaction of the dislocation with the elastic field it produces. In the case of an infinite periodic row of obstacles of diameter D, two dislocation branches on both sides of an obstacle can have their stress fields interact very strongly through so-called "dipole interactions", which will help the Orowan bypassing mechanism by affecting the critical shape of the branches and thus lowering the associated critical stress. Bacon et al. showed that this interaction could be accounted for by correcting the Orowan formula with the logarithm of the harmonic radius $D' = (D^{-1} + L^{-1})^{-1}$ of the obstacle. Additionally, using Kocks statistical theory for random array of penetrable obstacles [40], they provided the following formula:

$$\tau_{\text{OB}} = \left(\frac{\ln D'/b}{\ln l/b}\right)^{3/2} \frac{\mu b}{l}\frac{\ln(l/b)}{2\pi}, \tag{23}$$

where $l = 1/\sqrt{DC}$ is the average spacing in the slip plane between obstacles of density C. In this formula, the Orowan term $\frac{\mu b}{l}$ has been corrected by $\frac{\ln(l/b)}{2\pi}$ to account for the loop self interaction and $\left(\frac{\ln D'/b}{\ln l/b}\right)^{3/2}$ accounts for the mutual dipole interactions and for the randomness of the obstacle row. More recent MD simulations [41,42] on the interactions between dislocations and rows of voids have given support to this model as it fits very well simulation data in the case of impenetrable precipitates, such as carbides, and still

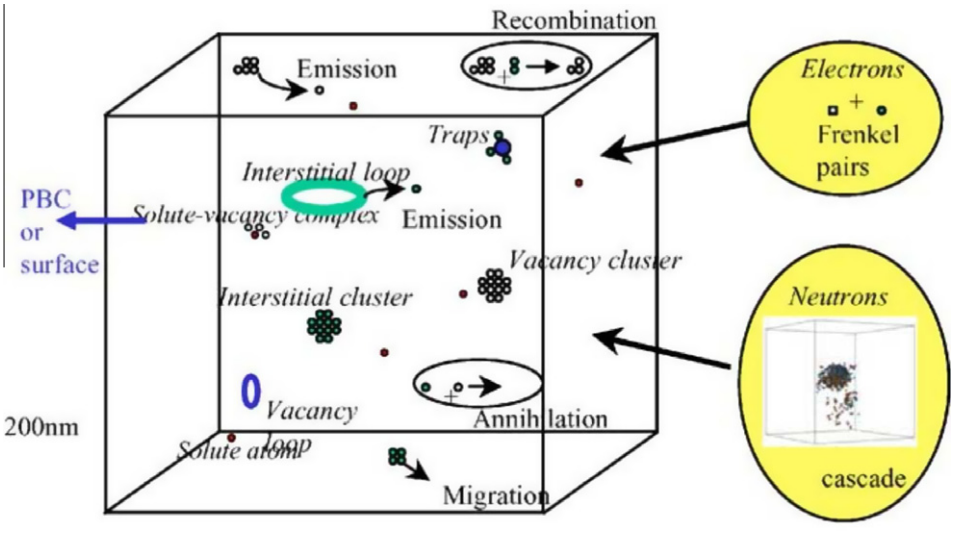

Fig. 4. Summary of the different events taking place in the OKMC simulation (PBC stands for periodic boundary conditions). At each simulation timestep, cascade insertions, emission, absorption or migration events involving defect clusters and solute atoms are chosen according to their respective probabilities. Figure from [17].

predicts reasonably well the hardening due to voids, which are shearable precipitates but appear to be stronger obstacles than unshearable ones.

The use of this formula to the cluster distributions (from the LONG_TERM submodule), implies the following additional assumptions:

- clusters are not space correlated, and their positions can be modeled as random,
- all clusters are Orowan precipitates (with a self and mutual dipole interaction correction from the Bacon et al. model). Note that this assumption may lead to an overestimation of the pinning force in the case of copper precipitates and interstitial clusters and to an underestimation in the case of voids which seem to constitute the major source of hardening in typical irradiation conditions,
- the diameter of the clusters D is taken as spherical in all cases. This is actually the case for cavities, precipitates and heterogeneous precipitates, which are known to form atmospheres around cavities, but it is not the case for interstitial loops. Nevertheless, this approximation may not be too severe as their number density is small compared to that of cavities, and, again, because loops are also much weaker obstacles than cavities.

As within our approximations, defects and solute atoms both constitute unshearable obstacles, let us denote as $n\prime = |n| + p$ the number of elements of an (n,p) cluster to be taken into account for the calculation its spherical diameter. Then the contribution of the random distribution of (n,p) clusters to the CRSS is:

$$\tau(n,p) = \sqrt{\frac{\ln D'/b}{\ln l/b}}\frac{\mu b}{2\pi l}\ln(D'/b), \tag{24}$$

The remaining task is now to integrate all the contributions to CRSS of the different cluster classes. DD simulations [37,38] suggested the use of the quadratic mixture law, as it is expected when summing up contributions from sources of hardening whose forces are of the same order of magnitude. The CRSS is finally calculated by integrating the contribution of all defect classes

$$\tau_c = \sqrt{\sum_{(n,p)}\tau(n,p)^2\Delta n\Delta p}. \tag{25}$$

To conclude, although the use of the Bacon et al. model requires several approximations, MD and DD simulations have shown that it accounts for the main features of the increase of CRSS due to irradiation. The main lack of this model is that it does not take into account the effect of temperature: the crossing of obstacles is thermally activated, which implies that thermal fluctuations can ease the crossing of small obstacles even without strain. Moreover, the contribution of weak 2D obstacles is not properly taken into account by this model for unshearable obstacles.

6.2. Mesoscopic simulation approach: the DUPAIR submodule

The DUPAIR code is an improvement of the original Foreman and Makin code [43,8] which implements an estimation method for the CRSS by modelling the glide of a single dislocation line in its slip system populated by obstacles. DUPAIR takes as an input the distribution of defect clusters from the LONG_TERM module and associates a pinning force to each of theses clusters depending on their size and type. A DUPAIR calculation is run for each of the cluster distributions corresponding to the various output times chosen.

For a given output time, the result corresponds to a tensile test that would be done at the reference temperature and the deformation rate, which play a role in the calculation of thermal activation term on the pinning forces.

Initially, the program randomly places in a 2D box the various type of defects according to their respective densities. A dislocation line is placed at the bottom of the box. An applied shear stress τ causes the segments of the single dislocation line to bow into a sequence of arcs of circles, each delimited by two pinning defects. The applied stress is increased incrementally until depinning occurs at some defect. Three different criteria are used for depinning:

- if the dislocation arc radius R_1 becomes smaller than half the defect distance $L/2$
- if the angle between the two dislocation branches at the defect position becomes smaller than a critical defined angle Θ_c
- if the norm of the resultant of the line–tensions on both sides of the obstacles, $\|\vec{T_1} + \vec{T_2}\|$, is larger than the pinning force F_P of the obstacle.

In practice, the last criterion is the most important. To be implemented, it requires the calculation of pinning forces of defects as a function of their type (voids, loops, precipitates or mixed clusters) and size. The building of the pinning forces database which DUPAIR relies on was the subject of dedicated publications [44] and it can be managed as a database. Three different models for the line-tension calculation are available:

The first model is a simple line-tension model. It supposes that the line-tension is independent of the character (edge, screw or mixed) of the dislocation segments. It is the original model used by Foreman and Makin to develop their code [43,8]. The basic equations for the model are given by the evaluation of the tension force and the shear force applied to a dislocation segment $d\mathbf{l}$:

$$d\mathbf{F} = \tau\mathbf{b}\wedge d\mathbf{l}, \tag{26}$$

$$T = \frac{\mu b^2}{2}, \tag{27}$$

$\mathbf{b}$ (resp. b) being the Burgers vector (resp. its norm), τ the applied shear stress, μ the shear modulus.

In this model, the line-tension is evaluated thanks to the Hirth and Lothe [45] approach:

$$T = \frac{\mu b^2}{4\pi}\frac{1+\nu-3\nu\sin^2\alpha}{1-\nu}\ln\frac{R}{r_0}, \tag{28}$$

where ν is the Poisson coefficient, α the angle between the Burgers vector and the dislocation segment, r_0 the core radius of the dislocation, and R the distance between two defects (cutoff distance, $R = L - 2r$, r being the mean radius of the defects). This model is more realistic since it takes into account the character of the segments of dislocations in their initial straight configuration.

The third model is an improvement of the second model, where R is given by a formula close to the harmonic radius proposed by Bacon *et al.* [46]:

$$R = \left(\frac{1}{\max(r_A, r_B)} + \frac{1}{L - r_A - r_B}\right)^{-1}, \tag{29}$$

r_A and r_B referring respectively to the radius of the pinning defects A and B, and L being the distance between their centres (as shown on Fig. 5).

After a depinning at some defect, the shape of the dislocation line is then accordingly reconfigured and the process of increasing the shear is restarted, until depinning occurs again. Periodic boundary conditions are used. The highest shear stress applied to allow the dislocation to glide is taken as the CRSS due to an array of obstacles.

To summarize, DUPAIR allows to estimate the CRSS resulting from a random array of shearable obstacles (whose force are inputs

of the code) and also takes into account in an elementary way the temperature dependence of the CRSS. In the next versions of the HARD module, the DD code MicroMegas will be integrated thus allowing to take into account the dislocation-forest interactions. This is necessary because although irradiation is not expected to modify their value significantly, it is necessary to evaluate all the various contributions to the hardening listed in Section 6 to estimate properly Eq. (21). Indeed, because the total CRSS is composed of sources of hardening of equivalent intensity, the linear mixture law used in the approximation Eq. (22) may not be valid, and the use of the quadratic mixture law would require to estimate all the main contribution to the hardening. This task was performed for case studies within the PERFECT project (see [47] for an overview) and should be fully integrated in the future versions of RPV-2.

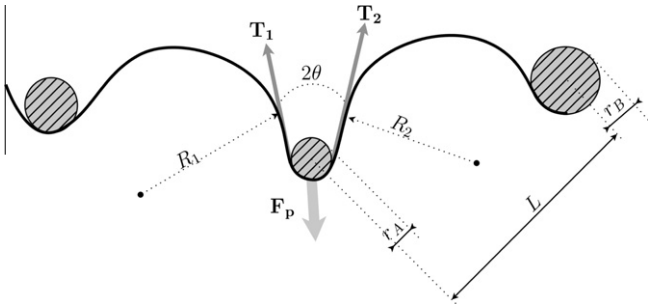

Fig. 5. Effect of shear strain on dislocations pinned on obstacles. Two dislocation arcs of respective radii R_1 and R_2 bowing between pinning obstacles of radii R_A and R_B. The central obstacle opposes a pinning force F_P to the line-tensions T_1 and T_2 resulting from the bowing of the two dislocation arcs.

7. Conclusion

In this article, we described the multiscale sequence of simulation modules that constitute the RPV-2 and INTERN-1 packages and which is summarized on Fig. 6. Starting from the neutron spectrum of the reactor, the calculation of the PKA spectrum was detailed. The underlying assumptions of the dpa calculation according to the NRT convention were shown to overestimate the actual dpa-rate which is more accurately calculated by MD. In practice, the source term is obtained from the PKA spectrum by decomposing damage energies onto a cascade database, which can be raw cascades for OKMC calculations or annealed cascades for the use of rate-theory calculations. Once the source term is computed, the determination of the irradiation microstructure by diffusion of the primary damage is followed at the chosen output time with the help of the LONG_TERM module. At this stage, either the rate-theory code MFVISC or the OKMC code LAKIMOCA can be chosen. Both of theses codes have been designed to tackle the complex problem of radiation induced heterogeneous segregation for the low copper contents of RPV steels, but further developments (for both mathematical issues such as solute conservation but also fundamental physical issues such as the description of the mobility of interstitials clusters in iron) will be necessary to be able to compare simulation and experimental results for Fe-Cu heterogeneous precipitates. At the end of the simulation sequence, the HARD modules use the clusters distributions to estimate the increase of CRSS due to irradiation. The increase of CRSS can be estimated, as a first approximation, to the CRSS associated to the irradiated microstructure. Two modules are available to estimate this quantity, the first one, the OrowanBacon module improves the usual formula for randomly dispersed unshearable precipitates by taking into account the self and mutual dipole interactions of dislocation branches on both sides of the obstacle. DD and MD simulations

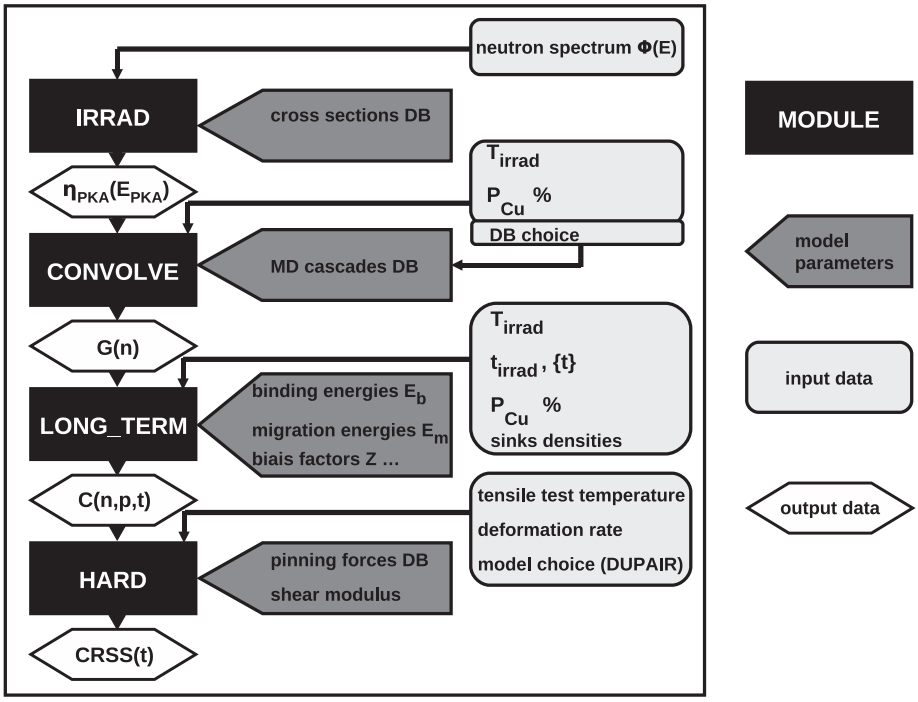

Fig. 6. Summary of the sequence of modules that constitute the RPV − 2 package. The role of the various databases (DB), sets of model parameters and user inputs described in this article is also reminded. The "core" of the package appears to be LONG_TERM module, which is fed by the source term calculation from the CONVOLVE module, i.e. the instantaneous defect production resulting from the cascade process initiated by neutrons irradiation. The LONG_TERM module models the various diffusion-controlled reactions between defects and produces as an output the defect cluster distributions for the set of output timesteps $\{t\}$ chosen by the user. Finally, the HARD modules estimates the CRSS associated to this set of cluster distributions.

support quite well these assumptions, at least for cavities. For interstitial loops, finite pinning forces must be considered, which can be done using the DUPAIR module. This Foreman and Makin formalism code, can also account for the influence of temperature on the CRSS in an elementary way. Nevertheless, the accuracy of CRSS calculation may be greatly improved in the follow up of the project by integrating DD, and thus properly treating the forest interactions and the thermal activation.

Acknowledgements

This work was partially funded by the European Project PERFECT (No. FI6O-CT-2003-508840). Drs. G. Monnet and S. Queyreau are gratefully acknowledged for their guidance on the use of analytical formulas for the HARD module. Dr. P. Olsson is also acknowledged for helpful comments.

Appendix A. The Kinshin-Pease model

The probability for displacement of atoms from their lattice sites depending on the incident neutron energy E_n is expressed by the displacement cross-section $\sigma_{\mathrm{DIS}}(E_n)$:

$$\sigma_{\mathrm{DIS}}(E_n) = \sum_k \int_{E_{\min}}^{E_{\max}} \sigma_k(E_n, E_{\mathrm{PKA}}) \nu(E_{\mathrm{PKA}}) dE_{\mathrm{PKA}}. \quad (30)$$

The last quantity appearing in Eq. (30), $\nu(E_{\mathrm{PKA}})$ is the so called "secondary displacement function", it represents the number of secondary displaced atoms by a PKA atoms of energy E_{PKA}. SPECTER uses the Kinshin-Pease model [48] for $\nu(E_{\mathrm{PKA}})$:

$$\begin{cases} \nu(E_{\mathrm{PKA}}) = 0, & E_{\mathrm{PKA}} \leqslant E_D. \\ \nu(E_{\mathrm{PKA}}) = 1, & E_D \leqslant E_{\mathrm{PKA}} \leqslant 2E_D \\ \nu(E_{\mathrm{PKA}}) = \frac{0.8 E_{\mathrm{dam}}(E_{\mathrm{PKA}})}{2E_D}, & E_{\mathrm{PKA}} \geqslant 2E_D. \end{cases}$$

These equations correspond to the following simple physical model:

- for PKA energies lower than E_D which is called the displacement threshold energy (about 40 eV in α-iron), no secondary displaced atoms are produced,
- for PKA energies between E_D and $2E_D$, one secondary atom is displaced,
- for PKA energies greater than $2E_D$, several secondary atoms are displaced.

Appendix B. Electronic loss model

In order to accurately estimate the energy which is available to produce secondary displaced atoms, the damage energy E_{dam}, one must correct the PKA energies with the electronic losses which result from the repulsive interaction between the electronic clouds of the PKA and the host material atoms. Lindhard's energy partitioning theory [49,16] provides one of the simplest models used to estimate electronic losses:

$$\begin{aligned} \xi &= \frac{E_{\mathrm{dam}}}{E_{\mathrm{PKA}}} = \frac{1}{1 + k_N g(\epsilon_N)}, \\ g(\epsilon_N) &= 3.4008 \epsilon_N^{1/6} + 0.40244 \epsilon_N^{3/4} + \epsilon_N, \\ k_N &= 0.1337 Z_1^{1/6} \left(\frac{Z_1}{A_1}\right)^{1/2}, \\ \epsilon_N &= \frac{A_2 T}{A_1 + A_2} \frac{a}{Z_1 Z_2 \epsilon^2}, \\ a &= \left(\frac{9\pi^2}{128}\right)^{1/3} a_0 (Z_1^{2/3} + Z_2^{2/3})^{-1/2}, \end{aligned}$$

where a_0 is the Bohr radius, ϵ is the electronic charge, E_{dam} is the damage energy in *keV*, A and Z are respectively the mass number and the atomic number of the PKA atom (index 1) and target atoms (index 2).

References

[1] S. Jumel, C. Domain, J. Ruste, J. Van Duysen, C. Becquart, A. Legris, P. Pareige, A. Barbu, V. Pontikis, J. de Phys. IV 10 (2000) 191.
[2] L. Malerba, E. van Walle, C. Domain, S. Jumel, J. Van Duysen, State of advancement of the international REVE project: computational modelling of irradiation-induced hardening in reactor pressure vessel steels and relevant experimental validation programme, in: Proceedings of ICONE 10: 10th International Conference on Nuclear Engineering ICONE10, 2002, p. 22260.
[3] S. Jumel, J. Van-Duysen, J. Nucl. Mater. 340 (2005) 125.
[4] S. Bugat, A. Zeghadi, G. Adjanor, J. Nucl. Mater. 392 (2009) 434–438.
[5] S. Bugat, J. El Gharib, J. Proix, A. Zeghadi, J. Nucl. Mater. 406 (2010) 187–192.
[6] C. Becquart, C. Domain, J. van Duysen, J. Raulot, J. Nucl. Mater. 294 (3) (2001) 274–287.
[7] C. Becquart, C. Domain, J. Raulot, to be published.
[8] A. Foreman, M. Makin, Can. J. Phys. 45 (1967) 511–517.
[9] L. Greenwood, SPECTER-ANL: Neutrons Damage Calculations for Materials Irradiations, ORNL report PSR-263.
[10] L. Greenwood, J. Nucl. Mater. 216 (1994) 29–44.
[11] M.J. Norgett, M.T. Robinson, I.M. Torrens, Nucl. Eng. Des. 33 (1975) 50–54.
[12] ASTM, Standard practice for characterizing neutron exposures in iron and low alloy steels in terms of displacements per atom (dpa), Annual Book of ASTM Standards 12.02 (1993) E693–E701.
[13] B. Radiguet, P. Pareige, A. Barbu, Nucl. Instrum. Methods Phys. Res. Sect. B: Beam Interact. Mater. Atoms 267 (2009) 1496–1499.
[14] K. Farrell, R. Stoller, P. Jung, H. Ullmaier, J. Nucl. Mater. 279 (1) (2000) 77–83.
[15] J. Massoud, A. Barbu, Comportement des matériaux dans le coeur des REP, Techniques de l'ingénieur (2008) BN3760.
[16] G. Was, Fundamentals of Radiation Materials Science, Springer, 2007.
[17] C. Domain, C. Becquart, L. Malerba, J. Nucl. Mater. 335 (1) (2004) 121–145.
[18] S. Jumel, J. Van-Duysen, J. Nucl. Mater. 328 (2–3) (2004) 151–164.
[19] R. Stoller, G. Odette, B. Wirth, J. Nucl. Mater. 251 (1997) 49–60.
[20] D. Bacon, A. Calder, F. Gao, V. Kapinos, S. Wooding, Nucl. Instrum. Methods Phys. Res. Sect. B: Beam Interact. Mater. Atoms 102 (1995) 37–46.
[21] R. Stoller, A.F. Calder, J. Nucl. Mater. 283–287 (Part 2) (2000) 746–752. 9th Int. Conf. on Fusion Reactor Materials.
[22] M. Miller, K. Russell, P. Pareige, M. Starink, R. Thomson, Mater. Sci. Eng. A 250 (1) (1998) 49–54.
[23] M. Mathon, A. Barbu, F. Dunstetter, F. Maury, N. Lorenzelli, C. de Novion, J. Nucl. Mater. 245 (2–3) (1997) 224–237.
[24] G. Odette, On the dominant mechanism of irradiation embrittlement of reactor pressure vessel steels, scriptametal.
[25] S.F. Fisher, J.E. Harbottle, U.B. Aldridge, Microstructure related to irradiation hardening in pressure vessel steels, in: Proceedings BNES Conference on Dimensional Stability and Mechanical Behaviour of Irradiated Metals and Alloys, BNES, 1984, p. 87.
[26] P. Pareige, B. Radiguet, A. Barbu, J. Nucl. Mater. 352 (1–3) (2006) 75–79. Proceedings of the E-MRS 2005 Spring Meeting Symposium N on Nuclear Materials.
[27] B. Radiguet, A. Barbu, P. Pareige, J. Nucl. Mater. 360 (2) (2007) 104–117.
[28] E. Meslin-Chiffon, Mécanisme de fragilisation sous irradiation aux neutrons d'alliages modèles ferritiques et d'un acier de cuve, Ph.D. Thesis, Univ. Rouen-CEA, 2007.
[29] E. Meslin, A. Barbu, L. Boulanger, B. Radiguet, P. Pareige, K. Arakawa, C. Fu, J. Nucl. Mater. 382 (2–3) (2008) 190–196. Proceedings of the Symposium on Microstructural Processes in Irradiated Materials.
[30] L. Mansur, J. Nucl. Mater. 216 (1994) 97–123.
[31] C. Becquart, C. Domain, Nucl. Instrum. Methods Phys. Res. Sect. B: Beam Interact. Mater. Atoms 202 (2003) 44.
[32] C. Fu, F. Willaime, P. Ordejón, Phys. Rev. Lett. 92 (2004) 175503.
[33] F. Willaime, C. Fu, M. Marinica, J. Dalla Torre, Nucl. Instrum. Methods Phys. Res. Sect. B: Beam Interact. Mater. Atoms 228 (2005) 92.
[34] E. Meslin-Chiffon, M. Lambretch, M. Hernández-Mayoral, F. Bergner, L. Malerba, P. Pareige, B. Radiguet, A. Barbu, D. Gómez-Briceño, A. Ulbritch, A. Almazouzi, J. Nucl. Mater. 406 (2010) 73–83.
[35] D. Kulikov, L. Malerba, M. Hou, Philos. Mag. A 86 (2006) 141–172.
[36] W. Young, E. Elcock, Proc. Phys. Soc. 89 (1966) 735–746.
[37] S. Queyreau, Etude des mécanismes d'écrouissage sous irradiation de la ferrite par simulations de dynamique des dislocations, Ph.D. Thesis, Univ. Pierre et Marie Curie-EDF, 2008.
[38] G. Monnet, Private communication.
[39] E. Orowan, Inst. Met. London 5 (1948) 451.
[40] U. Kocks, Can. J. Phys. 45 (1967) 737–755.
[41] Y. Osetsky, D. Bacon, J. Nucl. Mater. 323 (2–3) (2003) 268–280. Proceedings of the Second IEA Fusion Materials Agreement Workshop on Modeling and Experimental Validation.
[42] Y. Osetsky, D. Bacon, Mater. Sci. Eng. A 400–401 (2005) 374–377. Dislocations 2004.
[43] A. Foreman, M. Makin, Dislocation movement through random arrays of obstacles, Philos. Mag. 13 (1966) 911.
[44] S. Jumel, J. Van Duysen, J. Ruste, C. Domain, J. Nucl. Mater. 346 (2005) 79.
[45] J. Hirth, J. Lothe, Theory of Dislocations, Mc Graw-Hill Book Company, 1968.

[46] D. Bacon, U. Kocks, R. Scattergood, Philos. Mag. 28 (1973) 1241–1263.
[47] G. Monnet, C. Domain, S. Queyreau, S. Naamane, B. Devincre, Atomic and dislocation dynamics simulations of plastic deformation in reactor pressure vessel steel, J. Nucl. Mater. 394 (2009) 174–181.
[48] G. Kinchin, R. Pease, Reports Progr. Phys. 18 (1955) 1–51.
[49] J. Lindhard, V. Nielsen, M. Scharff, P. Thomsen, Mat. Fys. Medd. Dan. Vid. Selk 33 (1963) 1.